11,10

Stability of Planar Slits in Multilayer Graphite Crystals

© A.V. Savin[1,2], A.P. Klinov[1]

[1] Semenov Federal Research Center of Chemical Physics of the Russian Academy of Sciences (FRC CP RAS), Moscow, Russia
[2] Plekhanov Russian University of Economic, Moscow, Russia

E-mail: asavin@chph.ras.ru

Received October 28, 2025
Revised November 8, 2025
Accepted November 17, 2025

Using a two-dimensional coarse-grained chain model, planar slits in multilayer graphite crystals are simulated. It is shown that when covering a linear cavity on the flat surface of a graphite crystal with a multilayer graphene sheet, an open (unfilled slit) can form only if the cavity width does not exceed a critical value L_o (for width $L > L_o$, only a closed state of the slit is formed, with the cavity space filled by the covering sheet). The critical width of the open slit L_o increases monotonically with the number of layers K in the covering sheet. For a single-layer cavity, there is a finite critical value of its width $L_o < 3$ nm, while for two- and three-layer cavities, the maximum width of the open slit increases infinitely with increasing K as a power function K^α with exponent $0 < \alpha < 1$. Inside the crystal, two- and three-layer slits can have stable open states at any width. For a slit with width $L > 7.6$ nm, a stationary closed state is also possible, in which its lower and upper surfaces adhere to each other. Simulation of thermal oscillations showed that open states of two-layer slits with width $L < 15$ nm are always stable against thermal oscillations, while wider slits at $T > 400$ K transition from the open to the closed state. Open states of three-layer slits are always stable against thermal oscillations.

Keywords: graphene, graphite, flat slits, molecular dynamics, coarse-grained model.

DOI: 10.61011/PSS.2025.11.62968.303-25

1. Introduction

Nanosize pores and capillaries are actively studied due to their importance for understanding of many natural phenomena and their potential application. Thus, they may transfer liquid with new properties, which are not possible at a larger scale [1]. Nanopores are used to study biophysics and chemistry of individual molecules [2]. To create smooth capillaries with precisely controlled dimensions, a method of their assembly was proposed on the basis of Van der Waals interaction [3] from two atomically flat sheets, separated by spacers of two-dimensional crystals [4]. Two-dimensional materials that were used were single-layer and multi-layer graphenes with precisely controlled number of layers [5]. Such assembly makes it possible to create structures that may be seen as flat empty slits with height of several atoms in a graphite crystal [6]. Such slits were used to study water transfer in the channels with the height from one [7] to several dozens atomic layers [5,8]. A programmable nanoliquid switch was proposed on the basis of such channels [9].

Internal cavities may also be used as pressure nanosensors [10–13]. Flat slits in the laminar structures may serve as effective optical waveguides [14]. Other options of using two-dimensional slits are given in the review [15].

When nanoslits are created in graphene and other lamellar materials, a problem of stability of these pores to the environmental exposure arises. Thus, for example, in one of the first papers the nanochannels with the height of one carbon atom layer were unstable and collapsed in the experiment [5]. In fact it was possible to only obtain nanochannels with height of two, three or more layers. As it was shown in a later paper, the inability to produce nanochannels with the height of one layer was related to the insufficiently precise treatment of graphite nanocrystal edges that caused channel closure [7]. In paper [9] a phenomenological model was proposed to describe the stability of nanoslits. In this model stability of pores is determined by the balance of Van der Waals interactions of the upper and lower surface of the pore, pore deformation energy upon its collapse, and also capillary pressure caused by nanocondensation of a solvent inside the channel. Even though this model makes it possible to obtain the results that agree quite well with the experiment, it pays little attention to the case of a few layers in the upper part of the pore (continual approximation is applied), and the effect of layers sliding and thermal fluctuations is not taken into account as well. In this paper due to the use of coarse-grained and full-atomic model of the graphene pore, the effect of these factors on the nanopore resistance will be taken into account in more detail.

Graphene sheets (nanoribbons) may bend easily and slide on each other, which makes it possible for them to fill the substrate irregularities [16]. Such high mobility of the sheets prevents formation of large flat cavities (slits) with the height of several layers, since due to the shift and bend the upper and lower layers of the cavity may come closer,

having filled its space [17]. In this paper, the maximum possible dimensions of the cavity will be determined using a two-dimensional coarse-grained chain model of a multi-layer crystal. It will be shown that the permissible dimensions depend on the quantity of the graphene sheets that form the cavity surface.

Section *2* describes a two-dimensional coarse-grained chain model of a multi-layer graphite crystal in the form of a system of parallel linear chains. In section *3* this model is used to find stationary states of flat slits formed when the cavity on the flat surface of the crystal is coated with a multi-layer graphene. In section *4* the flat slits inside the graphite crystal are modelled, and in section *5* their resistance to thermal vibrations is analyzed. In section *6* modeling using full-atomic 3D models is carried out to test the obtained results. The main conclusions are presented in the section 7.

2. Chain model of multi-layer graphene

A graphene sheet is an elastically isotropic material, its longitudinal and flexural rigidity wealky depend on its chirality. Therefore, for certainty let us consider the sheet deformations in the zigzag direction; see Figure 1, *a*.

Let the sheet lie in plane xy of a three-dimensional space in its ground state. In direction of axis x (in zigzag direction) the sheet is a periodical structure with a pitch of $a_x = r_c \cos(\pi/6)$, where $r_c = 1.418$ Å — equilibrium length of valent bond C–C. Translational cells of this structure form atoms located along the lines parallel to axis y. If the movements of the graphene sheet are considered, when the atoms on one vertical line move synchronously, the sheet dynamics may be described as the displacement of the beads of the linear chain of atoms in plane xz; see Figure 1, *b*. Here every bead describes displacements of all atoms of the sheet located on a single vertical line (all atoms with the same coordinates x, z). Such two-dimensional chain model was first used to model the dynamics of carbon nanoribbon rolls [18,19] and folds in a graphene sheet on a flat substrate [20].

The Hamiltonian of such chain system has the following form

$$H = \sum_n \left[1/2\, M_c(\dot{u}_n, \dot{u}_n) + V(r_n) + U(\theta_n)\right], \qquad (1)$$

where index n specifies the number of the chain bead, $M_c = 12m_p$ — chain bead mass (carbon atom mass), $u_n = (x_n, z_n)$ — vector specifying the position of the nth bead, $r_n = |v_n|$ — distance between the adjacent beads n and $n+1$ (vector $v_n = u_{n+1} - u_n$), θ_n — angle between the adjacent beads of the chain (angle between vectors v_n and $-v_{n-1}$).

The longitudinal rigidity of the chain is described by a harmonic potential

$$V(r) = 1/2\, K_r (r - a)^2, \qquad (2)$$

where $a = a_x = 1.228$ Å — chain pitch, $K_r = 405$ N/m — the inter-bead interaction stiffness. The flexural rigidity of the chain is described with the following potential

$$U(\theta) = \varepsilon_\theta [\cos(\theta) + 1], \qquad (3)$$

where cosine of nth angle is $\cos(\theta_n) = -(v_{n-1}, v_n)/r_{n-1} r_n$, energy is $\varepsilon_\theta = 3.5$ eV. At these values of K and ε_θ the dispersion curves of the chain match best the dispersion curves of longitudinal and flexural oscillations of the flat graphene nanoribbon [18].

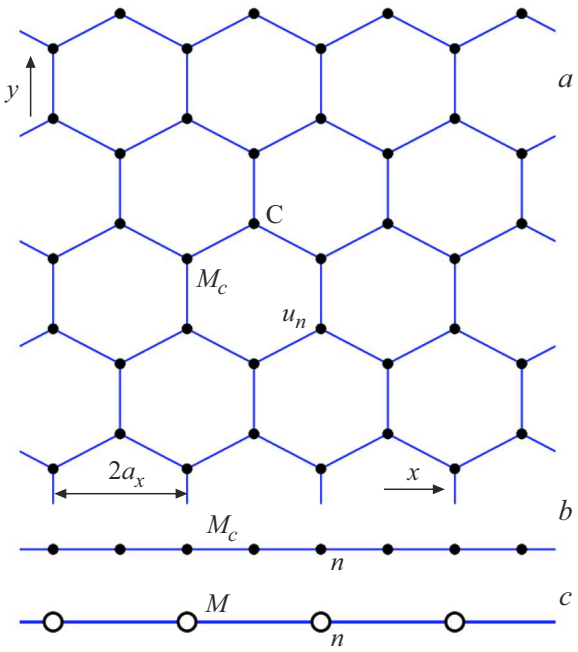

Figure 1. Schematic of the two-dimensional chain model construction for (*a*) a flat graphene sheet in plane xy (u_n — vector of coordinates of the nth carbon atom). The model of the chain (*b*) with a pitch of $a = a_x$ and (*c*) $a = 2a_x$ (n — number of the chain link, M_c — carbon atom mass, $M = 2M_c$ — united atom mass).

In the chain model, multilayer graphene sheet corresponds to a system of parallel chains (Fig. 2) with the Hamiltonian

$$H = \sum_{k=1}^{K} \sum_{n=1}^{N} 1/2\, M_c(\dot{u}_{n,k}, \dot{u}_{n,k}) + E_1 + E_2, \qquad (4)$$

where index k specifies the chain number, and n — the bead number. The vector $u_{n,k} = (x_{n,k}, z_{n,k})$ specifies the coordinates of nth bead of kth chain (K — number of chains, N — number of links per chain).

The first term in the Hamiltonian (4) specifies the kinetic energy of the molecular system, the second term describes the potential energy of the chains

$$E_1 = \sum_{k=1}^{K} \sum_{n=1}^{N} \left[V(r_{n,k}) + U(\theta_{n,k})\right], \qquad (5)$$

where the distance between the adjacent beads of the chain $r_{n,k} = |v_{n,k}|$ (vector $v_{n,k} = u_{n+1,k} - u_{n,k}$), cosine of the valence angle $\cos\theta_{n,k} = -(v_{n-1,k}, v_{n,k})/r_{n-1,k} r_{n,k}$.

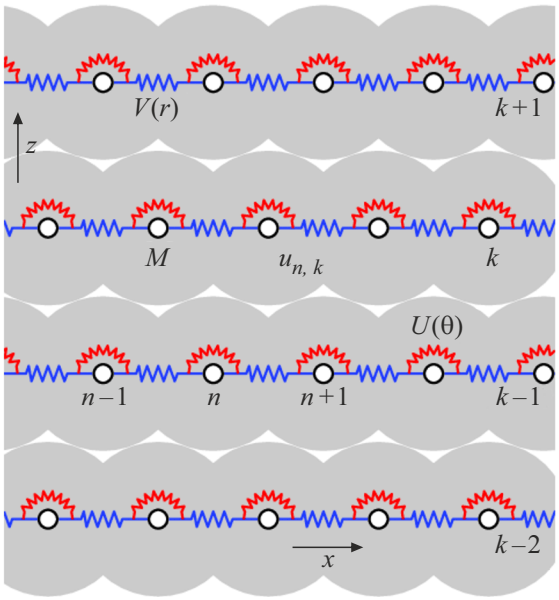

Figure 2. The chain model of the multilayer graphene, k — number of the chain (sheet layer), n — number of the chain bead (vector $u_{n,k}$ specifies the coordinates of the bead n, k), M — the bead mass. The potential $V(r)$ describes longitudinal rigidity, and $U(\theta)$ — flexural rigidity of the chain. Grey circles show Van der Waals radii of chain beads.

The third term

$$E_2 = \sum_{k_1=1}^{K-1} \sum_{k_2=k_1+1}^{K} \sum_{n_1=1}^{N} \sum_{n_2=1}^{N} W(r_{n_1,k_1;n_2,k_2}), \qquad (6)$$

describes weak non-valent (Van der Waals) interchain interactions, $r_{n_1,k_1;n_2,k_2}=|u_{n_2,k_2}-u_{n_1,k_1}|$ — the distance between the beads of chains (n_1, k_1) and (n_2, k_2). Energy of interaction may be described with high accuracy by Lennard–Jones potential (5,11)

$$W(r) = \varepsilon_0[5(r_0/r)^{11} - 11(r_0/r)^5]/6, \qquad (7)$$

with equilibrium bond length $r_0 = 3.61$ Å, energy of interaction $\varepsilon_0 = 0.0083$ eV [20].

Homogeneous state of the multilayer graphene (Figure 2) is set by the coordinates

$$\{u^0_{n,k} = (x^0_{n,k}, z^0_{n,k})\}^{N,K}_{n=1,k=1},$$

where $x^0_{n,k} = na$ for odd k and $x^0_{n,k} = (n + 1/2)a$ for even k, $z^0_{n,k} = kh_0$, $h_0 = 3.352$ Å — distance between adjacent chains (layers). To model an infinite graphene, it is convenient to use periodic boundary conditions, and for the end-size graphene — free boundary conditions.

To find the ground state, it is necessary to solve the problem for a minimum of potential energy of the molecular system

$$E = E_1 + E_2 \to \min : \{u_{n,k}\}^{N,K}_{n=1,k=1}. \qquad (8)$$

Table 1. Changes in the chain model parameters as the chain pitch increases d times (ΔE — pinning energy)

d	a	M	K_0 (N/m)	ε_θ (eV)	ε_0 (eV)	r_0 (Å)	ΔE (meV)
1	a_x	M_c	405.0	3.500	0.0083	3.610	0.1
2	$2a_x$	$2M_c$	202.5	1.750	0.0316	3.673	4.3
2.129	da_x	dM_c	190.2	1.644	0.0352	3.694	6.0

The minimization problem (8) was solved numerically by the conjugate gradient method [21,22]. For a system of chains corresponding to the crystal graphite, the distance between the adjacent chains (layers) is $h_0 = 3.352$ Å, and energy of interaction of one chain bead with the adjacent chain $E_0 = -52$ meV. Here, in order to shift the chain by one period, it is necessary to overcome an energy barrier $\Delta E = 0.1$ meV for every bead. To compare the energy of adhesion and pinning per atom calculated in the approximation of the density functional theory (DFT), they are $E_0 = 49$ meV, $\Delta E = 6$ meV, respectively [23]. Therefore, the two-dimensional chain model describes quite well the energy of interaction of the graphite sheets, but due to very low energy of pinning ΔE it makes it possible for the chains to practically freely slide one against another. In three-dimensional models, when the energy of atom interaction between the adjacent layers of graphene is described with the Lennard–Jones potential (6,12) [24] the assessments of the pinning energy per atom are low $\Delta E = 0.43$ meV. Precise agreement with the data from the DFT may be obtained in the models with the Kolmogorov–Crespi potential for interlayer interactions of atoms [23,25,26]. This potential takes into account the dependence of the interaction energy on the mutual orientation of normals to the graphene sheet, which makes it possible to describe the energy sliding surfaces in more detail.

One can increase the pinning energy in the chain model by increasing the chain period a (at the expense of using of more coarse-grained chain). Let us introduce the parameter of discretness $d = a/a_x$. To maintain the linear density, longitudinal and flexural rigidity when increasing the chain pitch d times, it is necessary to increase the bead mass d times, and to decrease the parameters K and ε_θ — down to d fold. The parameters of the potential (7) must be changed in order to preserve the distance between the adjacent chains h_0 and energy of their interaction E_0 per the chain length a_x in the ground state. The specific values of the changed parameters are given in Table 1. Of course, as the chain discreteness increases, the positions of beads no more correspond to positions of carbon atoms of the graphene sheet, but in the continual approximation the chain deformations with continue to correspond to the sheet deformations.

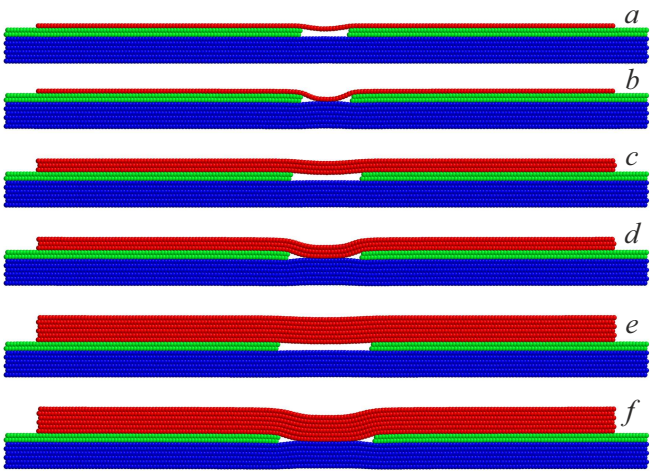

Figure 3. Stationary state of two-layer slit ($K_g = 2$) with width $L_x = (N_g + 1)a$, coated with K-layer graphene, at (a) $N_g = 15$, $K = 1$; (b) $N_g = 16$, $K = 1$, (c) $N_g = 22$, $K = 3$, (d) $N_g = 23$, $K = 3$, (e) $N_g = 29$, $K = 6$, (f) $N_g = 30$, $K = 6$. Red indicates the upper part of graphene, green — substrate sheets participating in the slit formation, blue — other substrate layers. A chain model with discretization parameter $d = 2$ (chain pitch $a = 2a_x = 2.456$ Å) was used. Only 8 upper layers from $K_s = 50$ layers are shown (number of beads per chain $N_s = 200$, $N = 180$).

3. Critical slit width depending on the thickness of the upper layer

To model the substrate with the linear cavity, let us first consider the system from $K_s = 50$ chains with periodic boundary conditions along axis x (number of beads in each chain $N_s = 200, 400$). To create a cavity from K_g the upper chains, let us remove it in the center of N_g of the beads; see Figure 3. The number of chains $K_g = 1, 2, 3$ determines the depth of the cavity $L_z = K_g h_0$, and the number of beads N_g — its width $L_x = (N_g + 1)a$. Let us then cover the substrate on top with the system from K parallel chains (number of links $N = 160, 320$). These chains correspond to K-layer graphene covering the cavity in the substrate, we will use the free boundary conditions for them. Therefore, the system of $K_a = K_s + K$ beads consisting of $N_a = K_s N_s - K_g N_g + KN$ links, we will model the linear cavity (slit) of $L_x \times L_z$ in the flat surface of graphene crystal coated on top with a finite multi-layer graphene.

To find the stationary state of this molecular system, it is necessary to numerically solve the problem for a minimum of its potential energy (8). To fix the slit position, let us fix the x-coordinates in the first external beads of the chains that form a slit. The solution to problem (8) showed that for $K_g = 1, 2, 3$ there is always a finite maximum possible width of the cavity $L_o = aN_g$, when the coating with multi-layer graphene will not result in filling of the slit space with the upper layer (the slit will remain in the stationary open state, where the coating graphene does not touch its bottom); see Figure 3, *a, c, e*. At larger width (at $L_x > L_o$) the slit space will always be filled with the upper layer (coating of the cavity results in the transition of the formed slit into the stationary closed state); see Figure 3, *b, d, f*. Here only the stationary state is possible, when the upper layer adjoins the bottom of the slit.

Note that such closed state is only possible for the slits with width of $L_x \geq L_c$. For narrow slits with $L_x < L_c$ there is only a stationary open state, and at $L_x \in (L_c, L_o)$ there are two stable stationary states with the empty and filled space of the slit. Here the slit (the coated cavity) is a bistable system. For wide slits with $L_x > L_o$ there is only a stationary state with the filled slit space. Dependence of the limit values of the slit width L_c and L_o on the number of graphene sheets K in the coating layer is provided in Table 2. As you can see from the table, for a two-layer chain these values are increasing monotonously as the number of K layers increases.

Figure 4 shows the dependence of the maximum width L_o on the number of graphene sheets K in the coating layer. As you can see from the figure, there is a limitation for a single-layer slit ($K_g = 1$) regarding the size of the unfilled (open) slit. Regardless of the number of K layers, the maximum width of the open slit is $L_o \leq 2.16$ nm when using a chain model with discreteness of $d = 1$, $L_o \leq 2.70$ nm at $d = 2$ and $L_o \leq 2.88$ nm at $d = 2.129$. For two- and three-layer slits ($K_g = 2, 3$) the maximum width of the open slit grows monotonously as a power-law function of the number of layers K:

$$L_o \sim K^{\alpha}, \quad \text{by} \quad K \to \infty.$$

For a two-layer slit the parameter is $\alpha = 0.17, 0.4$, and for a three-layer one — $\alpha = 0.22, 0.52$ (the values were obtained using a model with chain discreteness of $d = 1$ and $d = 2, 2.129$). Therefore, the increase of the discreteness parameter d causes the increase of the maximum slit width L_o. This width depends on the ability of the top layer to fill the slit, which is related to the ability of the longitudinal motion of this layer edges. As d increases, such ability decreases, since the pinning energy increases.

Note that the limit value of slit width L_o does not depend on the length of the coating chain $L = (N - 1)a$, if $N \gg N_g$. Thus, at $K_g = 2$, $K = 1$, the value $L_o = 3.93$ nm ($N_g = 15$) is obtained at $N = 90, 180, 360$, and at $N = 45$ the width is $L_o = 3.68$ nm ($N_g = 14$), at $N = 25$ the width is $L_o = 3.44$ nm ($N_g = 13$).

Table 2. Dependence of limit values of L_c, L_o slit width on the number of K graphene sheets in the coating layer for a two-layer slit ($K_g = 2$, $d = 2$)

K	1	2	3	4	6	8	10	14	20	30
L_c (nm)	3.17	3.42	3.67	3.91	4.16	4.41	4.66	5.15	5.40	5.64
L_o (nm)	3.93	4.67	5.65	6.39	7.37	8.35	9.34	10.56	12.28	14.00

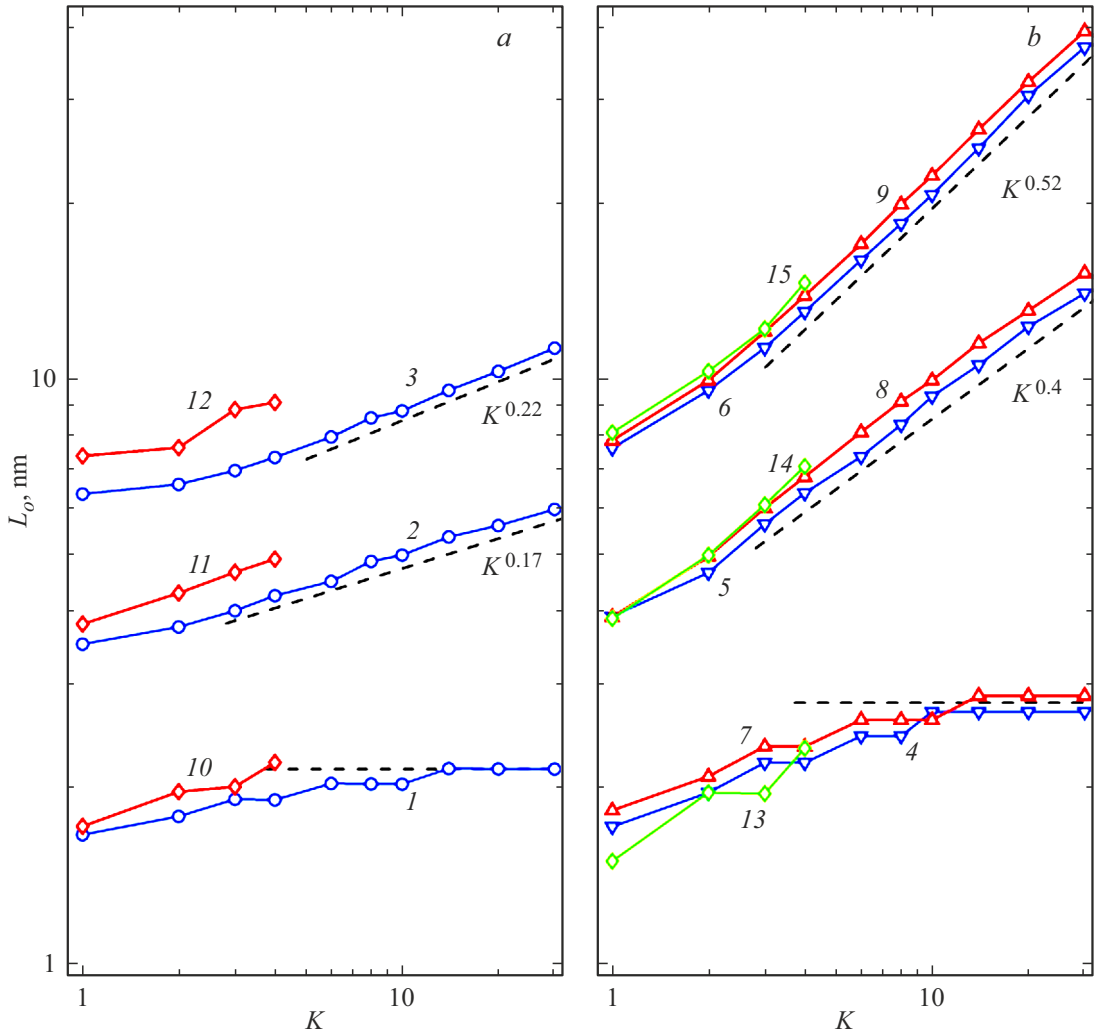

Figure 4. Dependence of maximum width of open state of L_o slit on the number of K graphene sheets in the coating layer. Within different models these dependences were calculated for a slit with height of one, two and three layers. The panel (a) compares the results of the initial two-dimensional model (parameter $d = 1$, curves *1,2,3*) with a full-atomic LJ-model (curves *10,11,12*). The panel (b) gives the values of maximum width in a two-dimensional model at $d = 2$ (curves *4,5,6*), at $d = 2.129$ (curves *7,8,9*), and also within a three-dimensional KC-model (curves *13,14,15*). Curves *1,4,7,10,13* provide dependence for a single-layer slit ($K_g = 1$), curves *2,5,8,11,14* — for a two-layer slit ($K_g = 2$), and *3,6,9,12,15* — for a three-layer slit ($K_g = 3$). Logarithmic axes are used, dotted lines show power-law dependences K^{α}.

The obtained dependences $L_o(K)$ make it possible to conclude that inside the graphite (multi-layer graphene) crystal the single-layer unfilled linear cavities (empty slits) may have the width of not more than 3 nm, and the width of the stable open two-layer and three-layer cavities is practically unlimited. Note that if the cavity in the substrate prior to its coating was previously filled with something, for example, with water, the size of such cavity is not limited. Here the molecules filling the cavity will prevent its collapse.

4. Slits inside a multi-layer crystal

To simulate the slits inside a multi-layer crystal, let us consider a system from $K = 100$ chains of $N = 200$ beads with periodic boundary conditions along both axes. For more certainty, let us further limit ourselves to use of the chain model with discreteness of $d = 2$.

Let us remove in $K_g = 1, 2$ adjacent chains the N_g beads, having thus created a slit with size of $L_x = (N_g + 1)a \times L_z = K_g h_0$ in the crystal. To find the stationary state of the slit, let us solve the problem of the minimum energy of the system (8). The numerical solution to the problem demonstrated that the single-layer slit in the crystal may stay in the unfilled state only at $N_g \leq 11$; see Figure 5. Therefore, the width of the open single-layer slit is always below 2.95 nm, which matches the estimate obtained in the previous section.

The solution to the problem (8) demonstrated that the open state of the two-layer slit is stable at any length (here the limit value is $L_o = \infty$). At $N_g \geq 30$

(at $L_x \geq L_c = 31a = 7.61\,\text{nm}$) there is also the closed stationary state of the slit, where its upper and lower surfaces adjoin each other; see Figure 6. Dependence of the energy difference of these stationary states of the $\Delta E = E_c - E_o$ slit on its width $L_x = (N_g + 1)a$ is shown in Figure 7. The energy difference grows practically linearly with the slit width increase. At $L_x < L_1 = 12.77\,\text{nm}$ the open state of the slit is more energetically favourable ($E_o < E_c$), and at $L_x > L_1$ the ground state will already be the closed state ($E_o > E_c$).

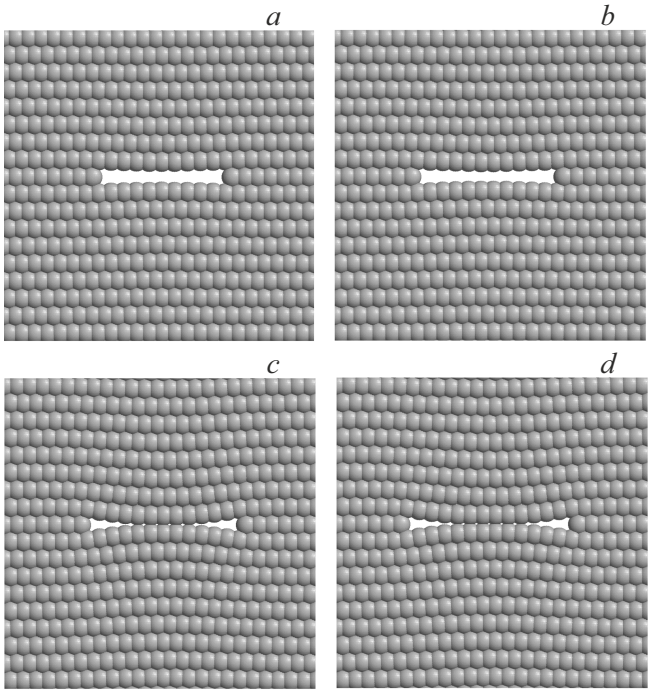

Figure 5. View of stationary state of single-layer slit in multi-layer crystal with width of $L_x = aN_g$ at $N_g = 10, 11, 12, 13$ (a, b, c, d). Chain pitch $a = 2a_x$ (chain discreteness $d = 2$).

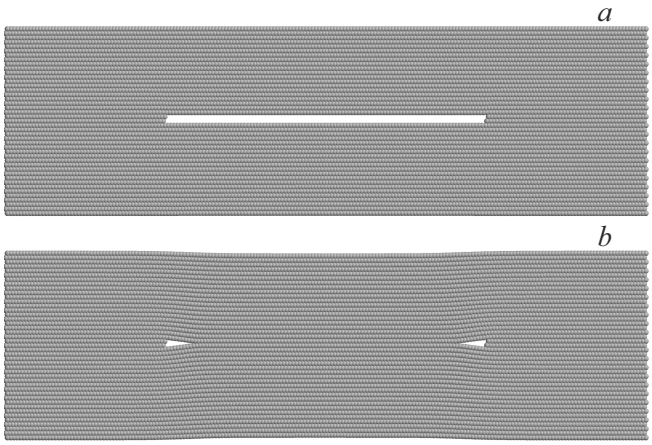

Figure 6. View of stationary state of two-layer (a) open and (b) closed slit in a multi-layer crystal with width of $L_x = 24.8\,\text{nm}$ ($N_g = 100$, chain pitch $a = 2a_x$).

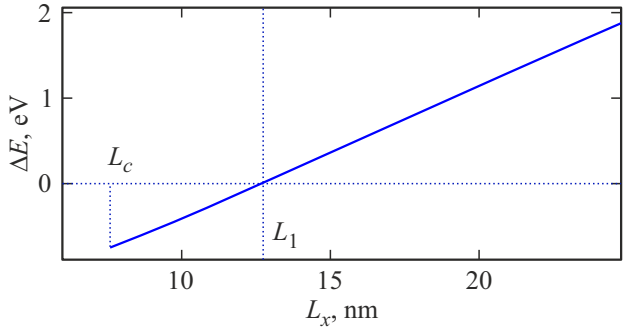

Figure 7. Dependence of energy difference $\Delta E = E_o - E_c$ of open and closed stationary state of two-layer slit in multi-layer crystal on its width L_x.

5. Impact of thermal fluctuations

To test the stability of the slit stationary states, let us conduct molecular-dynamic simulation at temperature of $T \leq 930\,\text{K}$. To simulate the thermal fluctuations of a multi-layer structure, it is necessary to numerically integrate the Langevin's system of equations

$$M\ddot{u}_{n,k} = -\frac{\partial H}{\partial u_{n,k}} - \Gamma M\dot{u}_{n,k} - \Xi_{n,k}, \qquad (9)$$

where index $k = 1, \ldots, K$ sets the chain number, index $n = 1, \ldots, N$ — chain bead number. Here $M = 2M_c$ — mass of a chain bead, $\Gamma = 1/t_r$ — friction coefficient (thermostat relaxation time $t_r = 10\,\text{ps}$),

$$\Xi_{n,k} = (\xi_{n,k,1}, \xi_{n,k,2})$$

two-dimensional vector of normally distributed random forces with correlation functions

$$\langle \xi_{n_1,k_1,i}(t_1)\xi_{n_2,k_2,j}(t_2)\rangle = 2Mk_\text{B}T\Gamma\delta_{k_1k_2}\delta_{n_1n_2}\delta_{ij}\delta(t_2 - t_1)$$

(k_B — Boltzmann constant, T — thermostat temperature).

In simulation we will use periodic boundary conditions with the fixed cell size. Therefore, for correct simulation it is necessary to take into account the thermal expansion of the system along axis z upon heating when setting the initial dimensions of the cell (the compression along axis x may be neglected). To study the change of the distance between the adjacent layers of graphene $\overline{h}(T)$, let us first consider the system from $K = 80$ chains from $N = 200$ links. Let us take along axis x (using index n) periodic boundary conditions with period Na, and along axis z (using index k) — free boundary conditions. Let us take the stationary state of the system from K parallel chains as the initial condition of the system of motion equations (9)

$$\{u_{n,k}(0) = u^0_{n,k}, \quad \dot{u}_{n,k}(0) = 0\}^{N,K}_{n=1,k=1}.$$

Let us numerically integrate the system of motion equations (9) by Verlet method [27] with integration step of $\Delta t = 1\,\text{fs}$. After equilibrium with the thermostat is achieved,

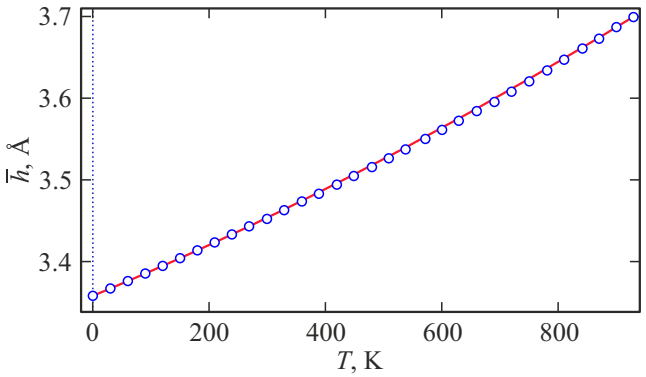

Figure 8. Dependence of average distance between adjacent chains $\overline{h}$ on temperature T. Markers provide values obtained numerically, the solid line corresponds to dependence (10).

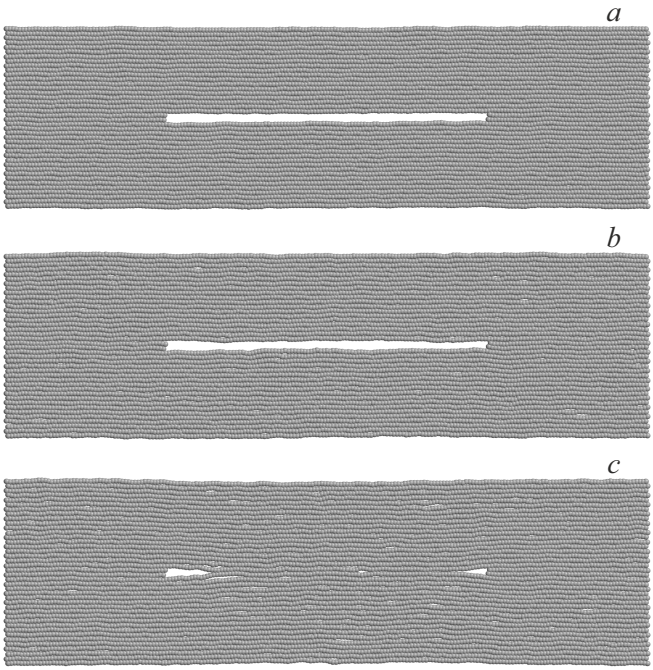

Figure 9. State of two-layer slit ($K_g = 2$, $N_g = 100$) in a multi-layer crystal at temperature (a) $T = 300$, (b) 510 and (c) 540 K. The configuration of the multi-layer system in the slit vicinity is shown at the moment of time $t = 5$ ns.

let us integrate the system for $t = 10$ ns and find the average value of the distance between the adjacent central chains $\overline{h}$.

Numerical simulation demonstrated that the thermal fluctuations result in increase of the distance between the adjacent chains, described with high accuracy by the following formula

$$\overline{h}(T) = h_0 + \alpha_1 T + \alpha_2 T^2, \qquad (10)$$

where $h_0 = 3.3576$ Å, $\alpha_1 = 3.0 \cdot 10^{-4}$ Å/K, $\alpha_2 = 7.3 \cdot 10^{-8}$ Å/K^2; see Figure 8.

To simulate the impact of thermal fluctuations on the slit shape, let us take the system from $K = 100$ parallel chains located at the distance of $\overline{h}(T)$ from each other. Let us take the chains with the bead number of $N = 200$, 400, 800. Along axis x we use the periodic boundary conditions with period of Na, and along axis z (using index k) — periodic boundary conditions with period of $K\overline{h}(T)$.

In virtue of instability of single-layer slits with width of $L > 3$ nm, slits with height of more than one layer that we will consider further are of greater interest.

To create a two-layer slit with width of $L = (N_g + 1)a$ we will remove N_g beads in two adjacent chains.

Numerical integration of the system of motion equations (9) demonstrated that the slit with width of $L < L_o = 15$ nm ($N_g < 60$) always remains in the open state at any temperature values. Wider slits at high temperatures will change to a closed state. Thus, at $N_g = 50$ the flat slit remained open at $T \le 930$ K for the entire time of numerical integration of $t = 5$ ns. At $N_g = 60$ the slit remains open at $T \le 600$ K (at higher temperatures the slit periodically changes from the open state to the closed one and back). At $N_g = 70$, 80, 100 and 200 ($L = 17.4$, 19.9, 24.8 and 49.4 nm) the slit remains open at temperature $T \le T_c = 510$, 630, 510 and 420 K, respectively. Here at $T > T_c$ the slit changes to the closed state and further remains in it; see Figure 9.

A three-layer slit ($K_g = 3$) is always stable to thermal fluctuations. Thus, at any temperature $T \le 930$ K it always remains in the open state.

6. All-atom simulation

It is natural to compare the predictions of the two-dimensional graphene model with a more detailed three-dimensional atomic model, where a separate particle corresponds to a carbon atom, but not an atom band with the width of da_x. Let us consider that the hydrogen atoms are attached to the carbon atoms on free edges of the graphene sheet. The group of these CH atoms will be considered by us as one (combined) atom of $13m_p$ mass.

Potential energy of the multi-layer graphene made of K nanoribbons on a flat substrate is:

$$E = \sum_{k=1}^{K}\sum_{n=1}^{N}[E_{n,k} + P(z_{n,k})] + \sum_{k_1=1}^{K-1}\sum_{k_2=k_1+1}^{K}\sum_{n_1=1}^{N}\sum_{n_2=1}^{N} W(r_{n_1,k_1;n_2,k_2}), \qquad (11)$$

where vector $u_{n,k} = (x_{n,k}, y_{n,k}, z_{n,k})$ specifies the coordinates of nth carbon atom of kth nanoribbon, N — number of atoms in each layer.

The first term of the sum (11) $E_{n,k}$ specifies the energy of interaction of nth atom of kth nanoribbon with the adjacent atoms of the nanoribbon (the deformations of valence bonds, valence and torsion angles are considered [28]). The potential

$$P(z) = e_0[\beta(h_z/z)^\alpha - \alpha(h_z/z)^\beta]/(\alpha - \beta), \qquad (12)$$

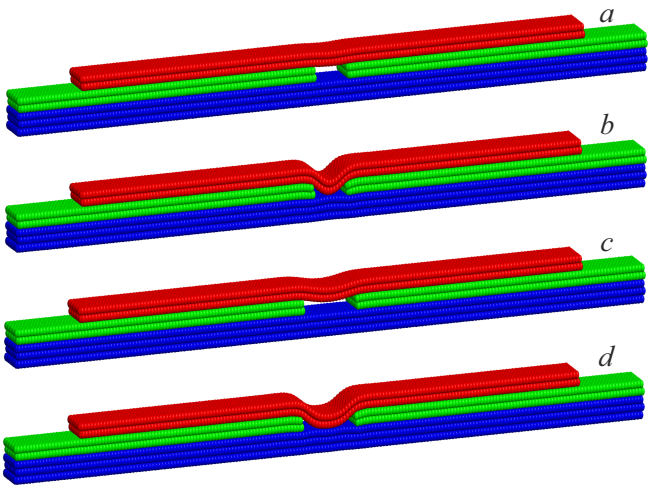

Figure 10. Stationary state of two-layer slit ($K_g = 2$), coated with two-layer graphene at width $L = 2.70\,\text{nm}$ ($N_g = 21$): (a) open and (b) closed state; at width $L = 4.30\,\text{nm}$ ($N_g = 34$): (c) open and (d) closed state. Red indicates the upper sheets of graphene, green — substrate sheets participating in the slit formation. LJ model is used.

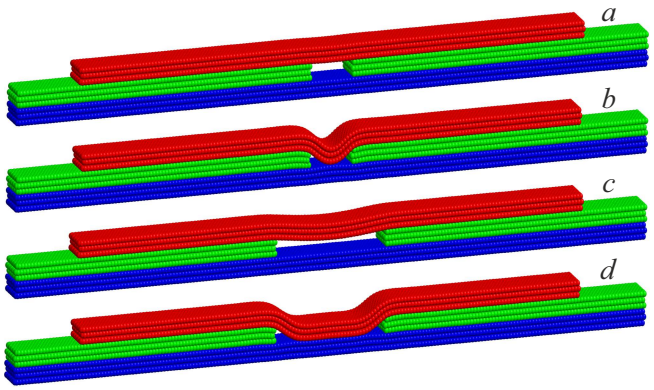

Figure 11. Stationary state of three-layer slit ($K_g = 3$), coated with three-layer graphene at width $L = 3.44\,\text{nm}$ ($N_g = 27$): (a) open and (b) closed state; at width $L = 8.72\,\text{nm}$ ($N_g = 70$): (c) open and (d) closed state. Red indicates the upper sheets of graphene, green — substrate sheets participating in the slit formation. LJ model is used.

describes the energy of interaction of the nanoribbon atom with the flat substrate $z \le 0$, formed by the surface of the graphite crystal, the interaction energy $e_0 = 0.0518\,\text{eV}$, equilibrium distance to the plane of the substrate $h_z = 3.37\,\text{Å}$, extent $\alpha = 10$, $\beta = 3.75$ [29].

The last term in formula (11) describes the energy of non-valence interaction of atoms in different layers, $r_{n_1,k_1;n_2,k_2} = |u_{n_2,k_2} - u_{n_1,k_1}|$ — distance between the atoms n_1, k_1 and n_2, k_2, potential

$$W(r) = \varepsilon_w\{[(r_w/r)^6 - 1]^2 - 1\}, \qquad (13)$$

where $\varepsilon_w = 0.002757\,\text{eV}$, $r_w = 3.807\,\text{Å}$ [24].

As it was described in section *2*, the above model with pairwise Lennard-Jones interactions of atoms (LJ-model) provides a lower pinning energy. Therefore, let us also consider a force field (KC-model), where the pinning energy of graphene sheets matches the results obtained by the DFT method [23]. In this force field the interaction of close atoms is determined by REBO [30] potential, and non-valence interactions of atoms from different layers — by Kolmogorov–Crespi potential [25]. The potential energy of the system was supplemented with a summand responsible for interaction with the substrate (12). The calculations by the energy minimization method for this model were conducted using LAMMPS suite [31].

Let us take as a substrate a multi-layer graphene from $K_s = 5$ nanoribbons, where direction „zigzag“ matches axis x, and direction „chair“ — axis y. Let us consider nanoribbons with size of $L_x = 2N_x a_x \times L_y = 3N_y r_c$, where $N_x = 200$, $N_y = 5$. Each nanoribbon will consist of $N_s = 4N_x N_y = 4000$ carbon atoms. To simulate the substrate, we will use the periodic boundary conditions with periods along axes x and y: $2N_x a_x = 49.12\,\text{nm}$ and $3N_y r_c = 2.127\,\text{nm}$.

To create a slit from $K_g = 1, 2, 3$ upper nanoribbons, let us remove in their center $N_g \times 4N_y$ atoms, having thus created a transverse cavity of width $L = (N_g + 1)a_x$; see Figure 10 and 11. Then we coated the cavity in the substrate with K-layer nanoribbon of the same width L_y, but shorter length $(2N - 1)a_x$ with a number of transverse cells $N = 160$. Here we will use the free boundary conditions along axis x, and along axis y — periodic boundary conditions. This three-dimensional molecular structure will correspond to the two-dimensional multi-layer structure considered in section 3.

To find the stationary state of the slit coated with multi-layer graphene, it is necessary to numerically solve the problem for a minimum of potential energy

$$E \to \min : \{u_{n,k}\}_{n=1,k=1}^{N_k,K_a}, \qquad (14)$$

where the total number of layers is $K_a = K_s + K$, N_k — number of atoms in kth layer (nanoribbon).

The numerical solution to the problem (14) demonstrated that for the number of layers participating in the formation of the slit $K_g = 1, 2, 3$ there is always the maximum possible width of the slit L_o, for which there is a stable stationary state with an open slit (in this state the upper layer will not touch the slit bottom); see Figure 10, *a,c* and 11, *a,c*. At larger width only the closed stationary state of the slit is possible, where the upper layer joins tightly the slit bottom — see Figure 10, *b,d* and 11, *b,d*. The closed stationary state only exists for the slits with width $L > L_c$, where the limit value of the slit is $L_c < L_o$. Therefore, for width $L < L_c$ there is only the open stationary state of the slit, at $L \in (L_c, L_o)$ there are simultaneously two stationary states (open and closed), and at $L > L_o$ the slit only has the closed state. The open stationary state is energetically more favourable only at the slit width of $L < L_1$, where the value is $L_1 \in (L_c, L_o)$. Specific values of the slit width L_c, L_1 and L_o are given in Table 3.

Table 3. Dependence of limit values of slit width L_c, L_1, L_o on the number of graphene sheets K in the coating layer for K_g-layer slit (values are given in nm, LJ-model is used)

K_g	K	1	2	3	4
1	L_o	1.72	1.97	2.09	2.21
2	L_c	2.09	2.46	2.58	2.82
2	L_1	2.58	2.95	3.19	3.44
2	L_o	3.81	4.30	4.67	4.91
3	L_c	2.09	2.46	2.58	2.82
3	L_1	3.56	4.05	4.42	4.79
3	L_o	7.37	7.61	8.37	9.09

As you can see from Figure 4, the three-dimensional LJ-model agrees well with the two-dimensional chain model ($d = 1$), and the KC-model — with the same model at $d = 2.129$. Values of the maximum width of the slit in the KC-model, as expected, somewhat exceed the estimates from the LJ-model. Differences in the pinning energy of two three-dimensional models also impact the deformation changes of the upper layer of graphene in slit collapse. Thus, in the KC-model with stronger pinning the collapse of the single-layer slit shifts edges of the upper layer relative to the middle layers by 0.1 Å in contrast to 1 Å for the LJ-model. Similar, but less pronounced differences are observed in collapse of the two-layer (shift by 0.4 Å vs. 1.3 Å) and three-layer slits (shift by 1.5 Å vs. 3.5 Å).

7. Conclusion

This paper refined the previously proposed two-dimensional chain model of multi-layer graphene [17]. By increasing the pitch of the chain $d = 2.129$ times and rescaling of interaction constants, the mechanical properties and the cohesion energy of graphene sheets were maintained, and the pinning energy was brought in compliance with the values calculated within the DFT simulation [23].

Formation of flat slits in multi-layer graphite crystals was simulated using a two-dimensional coarse-grained chain model. It was shown that the multi-layer graphene coating of the linear cavity on the flat surface of the graphite crystal may lead to formation of an open (unfilled) slit only at cavity width not exceeding the limit value L_o. At larger width of the cavity (at $L > L_o$) the upper layer of graphene due to bend and shift of the edges fully adjoins its bottom, forming the closed (collapsed) state of the slit. The closed state is only possible at the slit width exceeding the threshold value $L_c < L_o$. Therefore, for the narrow slits with width of $L < L_c$ only the open stationary state is possible. For the slits of medium sizes $L \in (L_c, L_o)$ there are two stable stationary states — open and closed. Here the slit (the coated cavity) is a bistable system. And for wide slits with $L > L_o$ there can only exist a closed stationary state with the space of the cavity filled with the coating top layer. The limit value of the width of the open slit L_o monotonously increases with the growth of the number of graphene sheets K in the coating layer. For the single-layer cavity there is a finite limit value of its width $L_o < 3$ nm, which does not depend on K. For two- and three-layer cavities the maximum width of the open slit grows as a power-law function as the K increases: $L_o \sim K^\alpha$, at $K \to \infty$ (index $0 < \alpha < 1$).

The conducted simulation demonstrated that the single-layer slit inside the graphite crystal may stay in the open (unfilled) state only at its width of $L < 3$ nm. Two- and three-layer slits here may have stable open states at any width (limit value of $L_o = \infty$). At $L > 7.6$ nm the two-layer slit may also remain in the stationary closed state, in which its lower and upper surfaces adjoin each other. The difference of energies in these stationary states grows linearly with the increase of the slit width. At width of $L < L_1 = 12.8$ nm the open state has lower, and at $L > L_1$ — higher energy.

Simulation of thermal fluctuations demonstrated that the open states of two-layer slits with width of $L < 15$ nm are resistant to thermal fluctuations at temperature of $T \leq 930$ K. Wider slits at $T > 400$ K transition from the open state to the closed state that is more energetically favourable. Open states of three-layer slits are always resistant to thermal fluctuations.

The conducted partial simulation of slits using three-dimensional full-atomic models confirmed the main results obtained using a two-dimensional chain model.

Funding

This study was supported by the Russian Science Foundation grant No. 25-73-20038, https://rscf.ru/project/25-73-20038/.

Conflict of interest

The authors declare that they have no conflict of interest.

References

[1] R.B. Schoch, J. Han, P. Renaud. Rev. Mod. Phys. **80**, 839 (2008).
[2] S. Howorka, Z. Siwy. Chem. Soc. Rev., **38**, 2360–2384 (2009).
[3] A. Geim, I. Grigorieva. Nature **499**, 419–425 (2013).
[4] K.S. Novoselov, D. Jiang, F. Schedin, T.J. Booth, V.V. Khotkevich, S.V. Morozov, A.K. Geim. PNAS **102**, *3*), 10451–10453 (2005).
[5] B. Radha, A. Esfandiar, F.C. Wang, A.P. Rooney, K. Gopinadhan, A. Keerthi, A. Mishchenko, A. Janardanan, P. Blake, L. Fumagalli, M. Lozada-Hidalgo, S. Garaj, S.J. Haigh, I.V. Grigorieva, H.A. Wu, A.K. Geim. Nature **538**, 222–225 (2016)
[6] A.K. Geim. Nano Letters **21**, *15*, 6356–6358 (2021). DOI: 10.1021/acs.nanolett.1c02591

[7] K. Gopinadhan, S. Hu, A. Esfandiar, M. Lozada-Hidalgo, F.C. Wang, Q. Yang, A.V. Tyurnina, A. Keerthi, B. Radha, A.K. Geim. Science **363** (6423), 145–148 (2019).
[8] A. Keerthi, S. Goutham, Y. You, P. Iamprasertkun, R.A.W. Dryfe, A.K. Geim, B. Radha. Nature Commun. **12**, *1*, 3092 (2021).
[9] N. Ronceray, M. Spina, V.H.Y. Chou, C.T. Lim, A.K. Geim, S. Garaj. Nat Commun **15**, 185 (2024).
[10] V. Sorkin, Y.-W. Zhang. J. Mol. Model. **17**, 2825–2830 (2011). DOI: 10.1007/s00894-011-0972-0
[11] A. Smith, S. Vaziri, F. Niklaus, A. Fischer, M. Sterner, A. Delin, M. Öastling, M. Lemme. Solid-State Electron. **88**, 89–94 (2013).
[12] M. Sanaeepur, A. Abedi, M.J. Sharifi. IEEE Trans. Electron Devices **64**, 1300–1304 (2017).
[13] S. Ahn, J. Jung, S. Choi, M. Son, Y. Hong, J.-C. Park. Sci. Rep. **7**, 12604 (2017).
[14] H. Ling, J.B. Khurgin, A.R. Davoyan. Nano Letters **22**, *15*, 6254–6261 (2022).
[15] J. Ma, K. Guan, Y. Jiang, Y. Cao, S. Hu. Nano Research **16** (3), 4119–4129 (2023).
[16] E. Han, J. Yu, E. Annevelink, J. Son, D. A. Kang, K. Watanabe, T. Taniguchi, E. Ertekin, P.Y. Huang, A.M. van der Zande. Nature Mater. **19**, 305–309 (2020).
[17] A.V. Savin, S.V. Dmitriev. Cavities in multilayer homo- and heterostructures. Physica E **151**, 115735 (2023).
[18] A.V. Savin, E.A. Korznikova, S.V. Dmitriev. Phys. Rev. B **92**, 035412 (2015).
[19] A.V. Savin, E.A. Korznikova, S.V. Dmitriev. Fizika tverdogo tela, **57**, *11*, 2278–2285 (2015). (in Russian).
[20] A.V. Savin, E.A. Korznikova, S.V. Dmitriev. Phys. Rev. B **99**, 235411 (2019).
[21] R. Fletcher, C. Reeves. Comput. J. **7**, *2*, 149–154, (1964).
[22] D.F. Shanno, K.H. Phua. ACM Trans. Math. Softw. (TOMS) **2**, *1*, 87–94 (1976).
[23] W. Ouyang, D. Mandelli, M. Urbakh, O. Hod. Nanoserpents: Nano Lett. **18**, *9*, 6009–6016 (2018).
[24] R. Setton. Carbon **34**, 69 (1996).
[25] A.N. Kolmogorov, V.H. Crespi. Phys. Rev. B **71**, 235415 (2005).
[26] T. Maaravi, I. Leven, I. Azuri, L. Kronik, O. Hod. J. Phys Chem C. **121**, 22826–22835 (2017).
[27] L. Verlet. Phys. Rev. **159**, 98 (1967)
[28] A.V. Savin, Yu.S. Kivshar, B. Hu. Phys. Rev. B **82**, 195423 (2010).
[29] A.V. Savin, O.I. Savina. Fizika tverdogo tela, (in Russian). **61**, *11*, 2257–2263 (2019).
[30] D.W. Brenner, O.A. Shenderova, J.A. Harrison, S.J. Stuart, S.B. Sinnott. J. Phys.: Condens. Matter **14** 783 (2002).
[31] S. Plimpton. J. Comput. Phys. **117**, *1*, 1–19 (1995).

Translated by M.Verenikina